

Fundamental Aspects of Near-Field Coupling Small Antennas for Wireless Power Transfer

Jaechun Lee, *Member, IEEE*, and Sangwook Nam, *Member, IEEE*

Abstract—A physical limitation on the power transfer efficiency between two electrically small antennas in the near-field range is presented. By using a Z-parameter which describes the interaction between two antennas for TE_{10}/TM_{10} spherical modes in connection with antenna parameters, the maximum power transfer efficiency and the optimum load impedance are shown as functions of the distance between two antennas, the radiation efficiency and the input impedance of the isolated antenna. The theory is verified by a simulation with a small helical antenna, which generates TE_{10} and TM_{10} modes, simultaneously.

Index Terms—Antenna efficiency, electromagnetic coupling, near fields.

I. INTRODUCTION

WIRELESS power transfer through coupled antennas in the near-field range is being widely used in radio frequency identification (RFID) systems. While RFID tags require a small amount of power for an instantaneous process, an increasing number of mobile electric devices are demanding higher amounts of wireless power transfer. The feasibility of this transfer depends on power transfer efficiency, and the results on this topic were reported recently [1]–[3]. As in earlier works, to estimate the power transfer efficiency of near-field coupling antennas, a numerical or analytical method can be used to solve the electromagnetic problem of the specified antennas by varying their positions. However, in view of such a system design, it is desirable that antennas are characterized as a few parameters and a closed-form of formula for the power transfer efficiency is given as a function of them like the Friis transmission formula between antennas in the far-field range. According to that purpose, the spherical mode representation is used to obtain a simple description of the problem, since the antennas used for wireless power transfer are electrically small and generate predominantly TE_{10} or TM_{10} spherical modes. Furthermore, the coupling properties between antennas are obtainable from the interaction theory between spherical modes in space [4]. A similar approach had been studied to investigate

the mutual coupling effect between adjacent antennas on the performance of an array antenna system [5], [6].

In this study, a simple and general model of antennas and coupling network among them in wireless power transfer system is presented based on the spherical mode theory. This enable us to evaluate system performance readily with a few parameters of antenna, and it informs us of the necessary parameters of antenna to achieve the power transfer efficiency required by an application. From the formulation, the physical limitation of the power transfer efficiency and the effect of the radiation efficiency on it are examined, and the optimum impedance for maximum power transfer efficiency is found.

In most applications, as in RFID systems, the relative orientation, or more generally, the relative polarization of the antennas will not coincide. The formula includes the case of different orientations using identical antennas; The case of different antennas can be treated with a similar method. The characteristics of coupling magnitude, that determines the power transfer efficiency, are analyzed in terms of the coupling coefficients between the spherical modes in parallel or orthogonal directions.

The theory is verified with an example of helical antenna. In addition, the optimum frequency of the power transfer efficiency is shown with this actual antenna in example, while an ideal lossless antenna shows the better power transfer efficiency at lower frequency.

II. THEORY

To obtain coupling network between antennas, first, their transmitting and receiving fields are expressed as spherical waves. Second, each antenna is represented by a scattering parameter between its feed port and spherical waves. Third, space between antennas is described as a Z-parameter among their spherical waves. Finally, antennas and space are cascaded into a two-port parameter between feed ports of two antennas. Throughout this study, $e^{j\omega t}$ time convention is assumed for the field quantities and suppressed.

A. Spherical Mode Representation of Antenna Model

The electric and magnetic fields outside an antenna can be expressed by spherical modes [8], [9]

$$\mathbf{E} = \eta^{1/2} \sum_{n,m,\epsilon} \left[a_{nm\epsilon}^+ \mathbf{M}_{nm\epsilon} + b_{nm\epsilon}^+ \mathbf{N}_{nm\epsilon} \right] \quad (1)$$

$$\mathbf{H} = \frac{j}{\eta^{1/2}} \sum_{n,m,\epsilon} \left[a_{nm\epsilon}^+ \mathbf{N}_{nm\epsilon} + b_{nm\epsilon}^+ \mathbf{M}_{nm\epsilon} \right] \quad (2)$$

Manuscript received October 30, 2008; revised June 18, 2009; accepted May 04, 2010. Date of publication August 30, 2010; date of current version November 03, 2010. This work was supported by the National Research Foundation of Korea (NRF) grant funded by the Korea government (MEST). (No. 2010-0018879).

J. Lee is with the Samsung Advanced Institute of Technology (SAIT), Yongin 449-712, Korea (e-mail: jcleee9@snu.ac.kr).

S. Nam is with the School of Electrical Engineering and INMC, Seoul National University, Seoul 151-742, Korea (e-mail: snam@snu.ac.kr).

Color versions of one or more of the figures in this paper are available online at <http://ieeexplore.ieee.org>.

Digital Object Identifier 10.1109/TAP.2010.2071330

where η is the wave impedance and $\mathbf{M}_{nm\epsilon}$, $\mathbf{N}_{nm\epsilon}$ are the spherical vector wave functions defined in Appendix A. $a_{nm\epsilon}^+$ and $b_{nm\epsilon}^+$ are the coefficients of $TE_{nm\epsilon}$ and $TM_{nm\epsilon}$ modes, respectively, whose superscripts, + and - indicate outward and inward traveling directions, respectively. The radiated power is written by

$$\begin{aligned} P_{rad} &= \frac{1}{2} \int_0^{2\pi} \int_0^\pi \operatorname{Re} [\mathbf{E} \times \mathbf{H}^*] r^2 \sin \theta d\theta d\phi \\ &= \frac{1}{2} \sum_{n,m,\epsilon} \left(|a_{nm\epsilon}^+|^2 + |b_{nm\epsilon}^+|^2 \right). \end{aligned} \quad (3)$$

Each spherical mode can be regarded as propagating in a waveguide of the unit characteristic impedance with its wave coefficient being $a_{nm\epsilon}^+$ or $b_{nm\epsilon}^+$.

Between these spherical modes and the feed port of the antenna, a S-parameter can be built [4]

$$\begin{bmatrix} \Gamma & \mathbf{R} \\ \mathbf{T} & \mathbf{S} \end{bmatrix} \begin{bmatrix} v \\ \mathbf{x} \end{bmatrix} = \begin{bmatrix} w \\ \mathbf{y} \end{bmatrix} \quad (4)$$

where Γ is the reflection coefficient at the feed port. \mathbf{R} , \mathbf{T} and \mathbf{S} are the receiving, transmitting and scattering coefficient matrices, respectively, for the spherical modes. v , w are the coefficients of the incident and reflected waves at the feed port, respectively. \mathbf{x} and \mathbf{y} are the coefficient vectors of the incident and reflected spherical modes, which contain $a_{nm\epsilon}^-$, $b_{nm\epsilon}^-$ and $a_{nm\epsilon}^+$, $b_{nm\epsilon}^+$, respectively.

Generally, antennas used for wireless power transfer are very small compared with wavelength, and are coupled in the near-field range. Such antennas predominantly generate the lowest-order spherical modes, i.e., TE_{1m} and TM_{1m} modes, which are represented as TE_{10} and TM_{10} modes, respectively, under properly rotated coordinates as shown in Appendix B. So we consider a small antenna assumed to

- radiate and receive only TE_{10} and TM_{10} modes, having no interaction with higher-order ($n > 1$) modes;
- have uniform phase of current distribution;
- be reciprocal.

The fields generated by the antenna are written in detail in Appendix A.

The input impedance of the single antenna is denoted as

$$Z_a = R_a + jX_a = R_a^{rad} + R_a^{loss} + jX_a \quad (5)$$

where R_a^{rad} and R_a^{loss} are the input resistances related with the radiated power into space and the loss in the antenna, respectively.

The radiation efficiency is defined by the ratio of the radiated power, P_{rad} , to the input power, P_{in}

$$\eta_{eff} = \frac{P_{rad}}{P_{in}} = \frac{R_a^{rad}}{\operatorname{Re}[Z_a]}. \quad (6)$$

The radiated power is divided into those of TE_{10} and TM_{10} modes

$$P_{rad} = P_{TE}^{rad} + P_{TM}^{rad} = \frac{1}{2} (R_{a,TE}^{rad} + R_{a,TM}^{rad}) I_{in}^2 \quad (7)$$

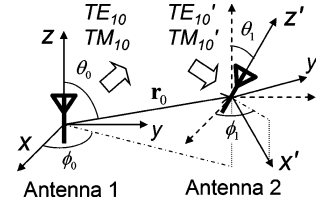


Fig. 1. Near-field coupling antennas modeling with TM_{10} and TE_{10} modes translation and rotation.

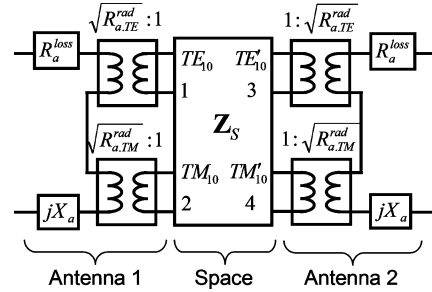


Fig. 2. Equivalent network between the input ports of two identical antennas.

where I_{in} is the input current of the antenna and $R_a^{rad} = R_{a,TE}^{rad} + R_{a,TM}^{rad}$.

The phases of the input current and the spherical mode coefficients are same since the current on the antenna is assumed to have a uniform phase and the spherical mode coefficients are determined by [8, Eq. (60)]

$$\begin{bmatrix} a_{nm\epsilon}^+ \\ b_{nm\epsilon}^+ \end{bmatrix} = -\eta^{1/2} \int_V \begin{bmatrix} \mathbf{M}_{nm\epsilon}^{(1)} \\ \mathbf{N}_{nm\epsilon}^{(1)} \end{bmatrix} \cdot \mathbf{J} dV \quad (8)$$

where \mathbf{J} is the current density and $\mathbf{M}_{nm\epsilon}^{(1)}$ and $\mathbf{N}_{nm\epsilon}^{(1)}$ are real-valued functions in free space as defined in Appendix A.

Then, from (3) and (7), the relation between the input current and the spherical mode coefficients is given as

$$\begin{bmatrix} a_{10}^+ \\ b_{10}^+ \end{bmatrix} = \begin{bmatrix} \sqrt{R_{a,TE}^{rad}} \\ \sqrt{R_{a,TM}^{rad}} \end{bmatrix} I_{in}. \quad (9)$$

This can be described as the transformer between antenna feed and spherical mode ports as depicted in Fig. 2. Its S-parameter representation with Z_0 of the feed port being Z_a^* is given by

$$\begin{bmatrix} 0 & \alpha & \beta & 0 & \cdots \\ \alpha & 1 - \alpha^2 & -\alpha\beta & 0 & \cdots \\ \beta & -\alpha\beta & 1 - \beta^2 & 0 & \cdots \\ 0 & 0 & 0 & 1 & \cdots \\ \vdots & & & & \ddots \end{bmatrix} \begin{bmatrix} v \\ a_{10}^- \\ b_{10}^- \\ \vdots \end{bmatrix} = \begin{bmatrix} w \\ a_{10}^+ \\ b_{10}^+ \\ \vdots \end{bmatrix} \quad (10)$$

where α and β , the transmitting coefficients for TE_{10} and TM_{10} modes, respectively, are

$$\alpha = \sqrt{\frac{R_{a,TE}^{rad}}{R_a}}, \quad \beta = \sqrt{\frac{R_{a,TM}^{rad}}{R_a}}. \quad (11)$$

These are related with the radiation efficiency as

$$\alpha^2 + \beta^2 = \eta_{eff}. \quad (12)$$

B. Space Description as the Relation of Spherical Modes in the Distance

Space can be seen as a four-port network between TE_{10}/TM_{10} spherical modes centered at each antenna positions as depicted in Fig. 2. This network parameter is obtained from the following relation among spherical modes with different origins and orientations, namely, the Addition theorem in Appendix C [9], [10]

$$\mathbf{M}_{10}(\mathbf{r}) = \sum_{\nu=1}^{\infty} \sum_{\mu=-\nu}^{\nu} A'_{\nu\mu,10} \mathbf{M}_{\nu\mu}^{(1)}(\mathbf{r}') + B'_{\nu\mu,10} \mathbf{N}_{\nu\mu}^{(1)}(\mathbf{r}') \quad (13)$$

$$\mathbf{N}_{10}(\mathbf{r}) = \sum_{\nu=1}^{\infty} \sum_{\mu=-\nu}^{\nu} A'_{\nu\mu,10} \mathbf{N}_{\nu\mu}^{(1)}(\mathbf{r}') + B'_{\nu\mu,10} \mathbf{M}_{\nu\mu}^{(1)}(\mathbf{r}') \quad (14)$$

where $\mathbf{r} = \mathbf{r}' + \mathbf{r}_0$, $\mathbf{r}_0 = (r_0, \theta_0, \phi_0)$, $r' < r_0$, and $A'_{\nu\mu,10}$, $B'_{\nu\mu,10}$ are the translation coefficients including rotation in Appendix C. $\mathbf{M}_{nm}^{(1)}$, $\mathbf{N}_{nm}^{(1)}$ are different from \mathbf{M}_{nm} , \mathbf{N}_{nm} in that the r -dependent function is $j_n(kr)$ instead of $h_n^{(2)}(kr)$, where $j_n(kr) = (1/2)h_n^{(1)}(kr) + (1/2)h_n^{(2)}(kr)$ is the spherical Bessel function of the first kind. $h_n^{(1)}(x)$ and $h_n^{(2)}(x)$ are the spherical Hankel functions of the first and second kind, corresponding to the inward and outward traveling wave, respectively. From (13), the wave coefficients at each coordinate can be set as $a_{10}^+ = 1$, $a_{10}^- = b_{10}^+ = b_{10}^- = 0$, $a_{10}'^+ = a_{10}'^- = A'_{10,10}/2$, $b_{10}'^+ = b_{10}'^- = B'_{10,10}/2$, where prime indicates origin at Antenna 2 position. By using the voltage and current definition with the unit characteristic impedance [11], Z-parameters are written by

$$Z_{TE,TE} = \frac{V_{TE}}{I_{TE}} = \frac{a_{10}^+ + a_{10}^-}{a_{10}^+ - a_{10}^-} = 1 \quad (15)$$

$$Z_{TM,TE} = \frac{V_{TM}}{I_{TE}} = \frac{b_{10}^+ + b_{10}^-}{a_{10}^+ - a_{10}^-} = 0 \quad (16)$$

$$Z_{TE',TE} = \frac{V_{TE}'}{I_{TE}} = \frac{a_{10}'^+ + a_{10}'^-}{a_{10}^+ - a_{10}^-} = A'_{10,10} \quad (17)$$

$$Z_{TM',TE} = \frac{V_{TM}'}{I_{TE}} = \frac{b_{10}'^+ + b_{10}'^-}{a_{10}^+ - a_{10}^-} = B'_{10,10} \quad (18)$$

where $I_{TM} = I_{TE}' = I_{TM}' = 0$. The remaining Z-parameters are obtained from (14) and by using reciprocity as

$$\begin{bmatrix} V_{TE} \\ V_{TM} \\ V_{TE}' \\ V_{TM}' \end{bmatrix} = \mathbf{Z}_s \begin{bmatrix} I_{TE} \\ I_{TM} \\ I_{TE}' \\ I_{TM}' \end{bmatrix} = \begin{bmatrix} 1 & 0 & A & B \\ 0 & 1 & B & A \\ A & B & 1 & 0 \\ B & A & 0 & 1 \end{bmatrix} \begin{bmatrix} I_{TE} \\ I_{TM} \\ I_{TE}' \\ I_{TM}' \end{bmatrix} \quad (19)$$

where $A'_{10,10}$, $B'_{10,10}$ are abbreviated as A , B .

C. Whole Coupling Network Between Two Antennas

We consider the case of using identical antennas; The case of different antennas can be treated with a similar method. Coupling network between two antennas is described by cascading networks of two antennas and space as depicted in Fig. 2. The whole network between two input ports of antennas can be obtained by conversion of Z-parameter of space in (19) into S-parameter and cascading it between S-parameters of antennas in (10), or by using scattering flow graphs in [4] with the S-parameters of antennas. It was found that two approaches yield

TABLE I
CHARACTERISTICS OF THE TRANSLATION COEFFICIENTS IN T IN TERMS OF CYLINDRICAL COMPONENTS AT $r_0 < 0.37$ WAVELENGTHS

Translated modes	Cylindrical components in T		
	\hat{z}	$\hat{\rho}$	$\hat{\phi}$
TE-TE (TM-TM)	max. at $\theta_0 = 0, \pi$	max. at $\theta_0 = \frac{\pi}{4}, \frac{3\pi}{4}$ zero at $\theta_0 = 0, \frac{\pi}{2}, \pi$	zero
Related coefficient	$A_{10,10}$	$A_{11e,10}$	
TE-TM (TM-TE)	zero	zero	max. at $\theta_0 = \frac{\pi}{2}$ zero at $\theta_0 = 0, \pi$
Related coefficient	$B_{10,10}$	$B_{11e,10}$	

the same result. Since the Z-parameter expression of the result is simpler than S-parameter expression, Z-parameter representation is used being written by

$$\mathbf{Z} = \begin{bmatrix} Z_a & \text{Re}[Z_a] \cdot T \\ \text{Re}[Z_a] \cdot T & Z_a \end{bmatrix} \quad (20)$$

where

$$T = \eta_{\text{eff}} \cdot A'_{10,10} + 2\alpha\beta \cdot B'_{10,10} \\ = \eta_{\text{eff}} \cdot \left(A'_{10,10} + \frac{2\sqrt{R_{a,TE}^{\text{rad}} R_{a,TM}^{\text{rad}}}}{R_{a,TE}^{\text{rad}} + R_{a,TM}^{\text{rad}}} B'_{10,10} \right). \quad (21)$$

T is the main factor of the maximum power transfer efficiency as will be shown in (29) and increasing its magnitude leads the maximum power transfer efficiency to 1. We can see that T is composed of two kinds of the translation coefficients, $A'_{10,10}$ and $B'_{10,10}$, which represent translation between the same kind of modes and different kind of modes, respectively, in (13) and (14). Each translation coefficient is separated into x, y and z-component as shown in (55) in Appendix C. Characteristics of them are rewritten as cylindrical components and summarized in Table I, showing three non-zero components. Thus T can be analyzed as a linear combination of three cylindrical components whose magnitude and combining ratio are determined by the position and orientation of Antenna 2, respectively.

The resulted Z-parameter is obtained under the assumption of only TE_{10} and TM_{10} modes generation and interaction. But this assumption becomes invalid when two antennas approach very close, because the magnitudes of higher order modes increase too large to neglect in the vicinity of an antenna owing to the faster increase of the higher order Hankel functions in their modes. So the Z-parameter deviates from the formula within a close distance between antennas, which will be shown with an example in Section IV.

III. MAXIMUM POWER TRANSFER EFFICIENCY AND OPTIMUM LOAD IMPEDANCE

From the Z-parameter, the input impedance of the transmitting antenna is given by

$$Z_{in} = Z_a - \frac{Z_{21}^2}{Z_a + Z_L} \quad (22)$$

where Z_L is the load impedance of the receiving antenna. The input power is

$$P_{in} = \frac{1}{2} \text{Re}[Z_{in}] |I_{in}|^2. \quad (23)$$

The power delivered to the load is

$$\begin{aligned} P_L &= \frac{1}{2} \text{Re}[Z_L] |I_L|^2 \\ &= \frac{1}{2} \text{Re}[Z_L] \left| \frac{Z_{21} I_{in}}{Z_a + Z_L} \right|^2. \end{aligned} \quad (24)$$

The power transfer efficiency is defined by

$$\text{PTE} = \frac{P_L}{P_{in}} = \frac{\text{Re}[Z_L]}{\text{Re}[Z_{in}]} \left| \frac{Z_{21}}{Z_a + Z_L} \right|^2. \quad (25)$$

The maximum power transfer efficiency can be found where

$$\frac{\partial \text{PTE}}{\partial \text{Re}[Z_L]} = 0, \quad \frac{\partial \text{PTE}}{\partial \text{Im}[Z_L]} = 0. \quad (26)$$

This yields the optimum load impedance and the maximum power transfer efficiency as

$$\text{Re}[Z_L^{opt}] = \text{Re}[Z_a] \sqrt{1 - \text{Re}[T^2] - \frac{1}{4} \text{Im}[T^2]^2} \quad (27)$$

$$\text{Im}[Z_L^{opt}] = \frac{1}{2} \text{Re}[Z_a] \text{Im}[T^2] - \text{Im}[Z_a] \quad (28)$$

$$\text{PTE}^{max} = \frac{|T|^2}{2 - \text{Re}[T^2] + \sqrt{4(1 - \text{Re}[T^2]) - \text{Im}[T^2]^2}} \quad (29)$$

where $T = Z_{21}/\text{Re}[Z_a]$. This can be also obtained from the simultaneous conjugate matching condition of a two-port network for the maximum transducer power gain [12, p. 619] as

$$Z_{in} = Z_L^*. \quad (30)$$

From (29), we can see that the maximum power transfer efficiency depends only on T as a function of the relative position and orientation of antennas, their radiation efficiency and the ratio between TE_{10} and TM_{10} modes.

In Fig. 4, the maximum power transfer efficiency with $\eta_{\text{eff}} = 1$ for four cases of antenna position and orientation are compared. The cases of (a), (c) and (d) also represent the three cases of maximum coupling by $A_{10,10}$, $A_{11\epsilon,10}$ and $B_{11\epsilon,10}$, respectively, in Table I. The result shows that the best performance in a range less than 0.3 wavelengths is obtained by placing the other antenna with parallel orientation at $\theta_0 = 0$.

In Table II, 2-dimensional patterns of the maximum power transfer efficiency with respect to the orientation of Antenna 2 at $r_0 = 0.1$ wavelengths and $\theta_0 = 0, \pi/4, \pi/2$ are illustrated. A radial and angular position within the circular pattern correspond to θ_1 and ϕ_1 , respectively, of the orientation of Antenna 2 as depicted in Fig. 3(b). Each pattern is separated into the cases of considering only one of three non-zero components in Table I separately in T , and compared with the original case where all components are combined in T . We can observe that at the position of Antenna 2 at $\theta_0 = 0$, only \hat{z} -component related with $A_{10,10}$ works, and away from the position at $\theta_0 = 0$, $\hat{\rho}$ -component related with $A_{11\epsilon,10}$ and $\hat{\phi}$ -component

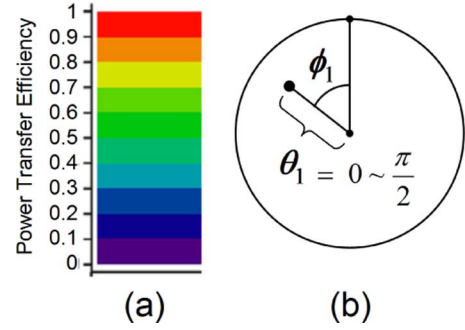


Fig. 3. (a) Legend and (b) 2-dimensional mapping of the orientation of Antenna 2 for the maximum power transfer efficiency pattern in Table II.

TABLE II
MAXIMUM POWER TRANSFER EFFICIENCY PATTERN WITH RESPECT TO
2-DIMENSIONAL MAPPING OF THE ORIENTATION OF ANTENNA 2 AT
 $r_0 = 0.1$ WAVELENGTHS

Antenna 2 position	Only one component considered			All components combination
	\hat{z} ($A_{10,10}$)	$\hat{\rho}$ ($A_{11\epsilon,10}$)	$\hat{\phi}$ ($B_{11\epsilon,10}$)	
$\theta_0 = 0$		zero	zero	
$\theta_0 = \pi/4$				
$\theta_0 = \pi/2$		zero		

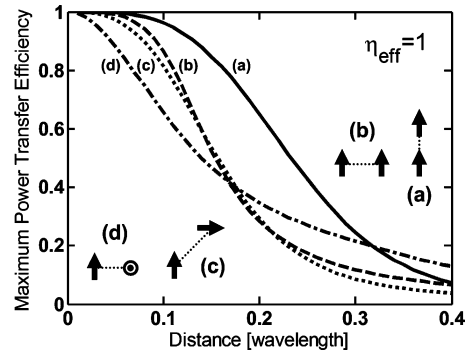


Fig. 4. The maximum power transfer efficiency with $\eta_{\text{eff}} = 1$ against the position and orientation of the opposite antenna at $(\theta_0, \theta_1, \phi_1 - \phi_0) =$ (a) $(0, 0, 0)$, (b) $(\pi/2, 0, 0)$, (c) $(\pi/4, \pi/2, 0)$, (d) $(\pi/2, \pi/2, \pi/2)$.

related with cross-coupling term, $B_{11\epsilon,10}$ in T affect the maximum power transfer efficiency pattern at $\theta_0 = \pi/4$ and $\pi/2$.

It is notable that the input reactance of the antenna has no effect on the maximum power transfer efficiency and only shifts the optimum load reactance in (28). So we will see the optimum load impedance of the antenna with $\text{Im}[Z_a] = 0$ as a standard. From (27) and (28), the optimum load impedance corresponding to Fig. 4 is plotted on the Smith chart in Fig. 5 as the optimum load reflection coefficient

$$\Gamma_L^{opt} = \frac{Z_L^{opt} - R_a}{Z_L^{opt} + R_a} \quad (31)$$

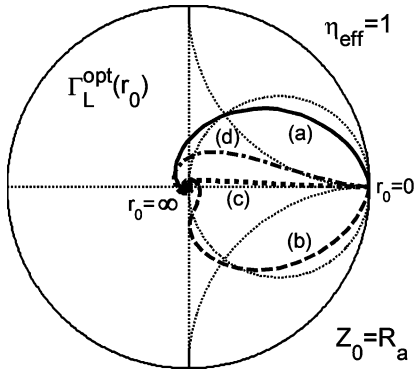


Fig. 5. The Smith chart representation of the optimum load impedances corresponding to Fig. 4 ($Z_0 = R_a$, $X_a = 0$).

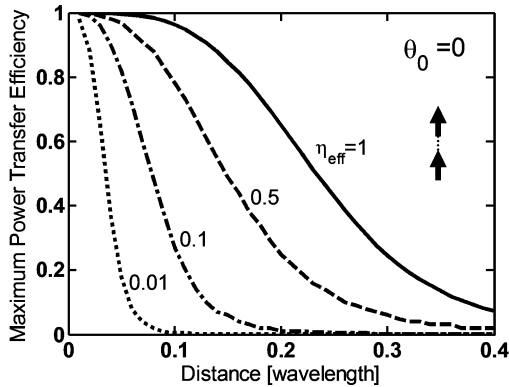


Fig. 6. The maximum power transfer efficiencies of antennas with different radiation efficiencies ($\eta_{\text{eff}} = 1, 0.5, 0.1, 0.01$) at $\theta_0 = 0$.

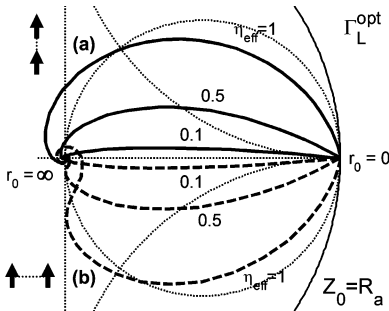


Fig. 7. The Smith chart representation of the optimum load impedances of antennas with different radiation efficiencies ($\eta_{\text{eff}} = 1, 0.5, 0.1$) at $\theta_0 = 0$ (solid), $\pi/2$ (dash) according to the distance between antennas.

where the characteristic impedance, Z_0 , is set as R_a . Fig. 5 exhibits various paths depending on cases, but common direction toward infinite load as the distance between antennas gets closer. So, the larger magnitude of load is proper at a closer distance. The dependence on the radiation efficiency as a crucial factor in the maximum power transfer efficiency is shown in Fig. 6. If we use an ideally lossless antenna ($\eta_{\text{eff}} = 1$), then lowering frequency achieves the higher transfer efficiency at a fixed distance. But since the radiation efficiency of an actual antenna under a given size decreases at the lower frequency, there may exist an optimum frequency as shown in the following example. As the radiation efficiency decreases, more variance is required for the optimum load resistance while less is required for the optimum load reactance as shown in Fig. 7.

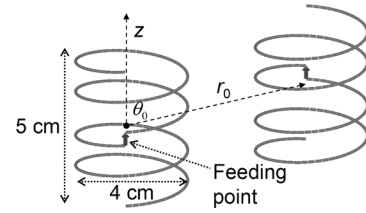


Fig. 8. Center-fed helical antennas (height = 5 cm, diameter = 4 cm, wire thickness = 1 mm, 4-turns, operating frequency = 300 MHz).

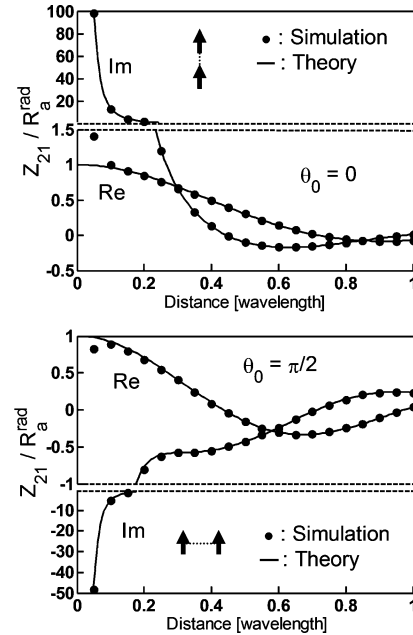


Fig. 9. Normalized Z_{21} of the helical antenna at $\theta_0 = 0, \pi/2$.

IV. EXAMPLE

To verify the theory, we compare the Z-parameters of an actual antenna with that in (20). A center-fed helical antenna is chosen as illustrated in Fig. 8 with 4 turns, 4 cm diameter, 5 cm height, and a copper wire thickness of 1 mm. The helical antenna consists of open-ended wires and acts both like a dipole and loop antenna. It generates both TE_{10} and TM_{10} modes and resonates by itself at about 295 MHz. We set the operating frequency at 300 MHz for the unit wavelength. Simulation is carried out using commercial software, FEKO, which is based on the method of moments. The input impedance of the single antenna, obtained by simulation, is $1.91 + j26.56 \Omega$ at 300 MHz. We assume the antenna is tuned to have zero reactance with a series capacitor. The radiation resistance is given as 1.47Ω from the simulation with a perfect electric conductor (PEC) wire. The radiation efficiency becomes 0.77 by (6). Z_{11} of the two antennas when close together is computed in Table III with normalization by the input impedance of the single antenna. It shows that Z_{11} in (20) becomes invalid in distances within 0.1 wavelengths, which is about twice the antenna size. This is because the assumption becomes invalid when two antennas approach very close as mentioned above. Z_{21} of the two antennas, normalized by the radiation resistance, is depicted in Fig. 9 in comparison with T/η_{eff} from (20) by the theory. It

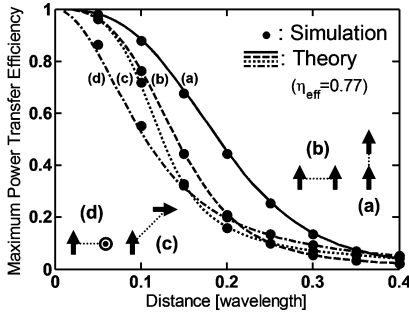


Fig. 10. The maximum power transfer efficiency of the helical antenna ($\eta_{\text{eff}} = 0.77$, frequency = 300 MHz) in four cases.

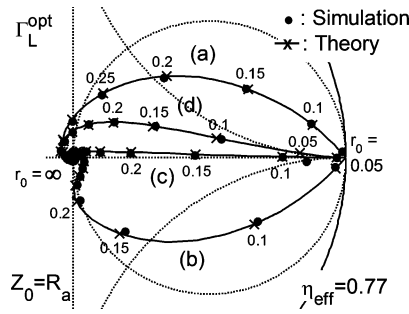


Fig. 11. The Smith chart representation of the optimum load impedances corresponding to Fig. 10.

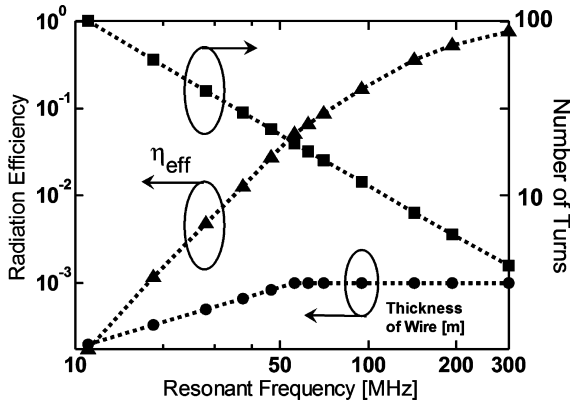


Fig. 12. Radiation efficiency of the helical antenna with different resonant frequency under the same size and corresponding number of turns and thickness of wire.

shows a good agreement in distance of more than 0.1 wavelengths and some deviation within 0.1 wavelengths similar to Z_{11} . Although the Z-parameter shows deviation from the theory when two antennas are very close, at that point, the maximum power transfer efficiency is already converging to 1, and thus does not deviate from the theory as shown in Fig. 10. The optimum load impedance in Fig. 11 also shows the validity of the theory. As mentioned above, to find out the optimum frequency for the maximum power transfer efficiency under the fixed size, the resonant frequency of the antenna is lowered by increasing the number of turns without increasing its size. Under the frequency of 50 MHz the thickness of wire is reduced to avoid the direct contact between wires. The radiation efficiency calculated by simulation in Fig. 12 shows a decrease at lower frequency as expected. From this, the distances required for the maximum power transfer efficiency of 50%, 70% and 90% are found in

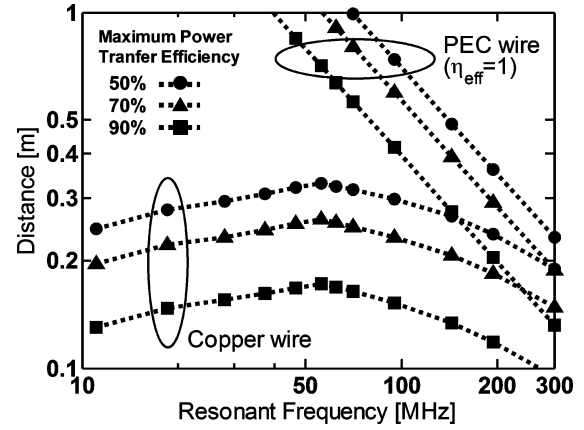


Fig. 13. Distance for the maximum power transfer efficiencies of 50% (○), 70% (△), and 90% (□) with the helical antenna and a lossless antenna ($\eta_{\text{eff}} = 1$).

TABLE III
NORMALIZED Z_{11} OF THE HELICAL ANTENNA

Distance [wavelength]	$\theta_0 = 0$		$\theta_0 = \pi/2$	
	$\frac{\text{Re}[Z_{11}]}{R_a}$	$\frac{\text{Im}[Z_{11}]}{X_a}$	$\frac{\text{Re}[Z_{11}]}{R_a}$	$\frac{\text{Im}[Z_{11}]}{X_a}$
0.05	1.291	2.39	0.939	1.332
0.1	1.023	1.016	0.98	1.004
0.15	1.01	1.001	0.993	1
0.2	1	1	0.997	1

Fig. 13 and shows the optimum frequency at around 56 MHz while an ideal lossless antenna with $\eta_{\text{eff}} = 1$ shows a continuous increase of the distance at lower frequency.

V. CONCLUSION

To simplify and generalize the wireless power transfer problem, an approximate Z-parameter has been built by relating TE₁₀ or TM₁₀ mode interaction with the antenna parameters. Using the Z-parameter, we have shown the maximum power transfer efficiency according to the radiation efficiency of the single antenna. The corresponding optimum load impedance has been plotted for reference. Although the Z-parameter shows deviation from the theory when two antennas are very close, the theory provides a helpful measure to estimate the power transfer efficiency of the near-field coupling antennas.

APPENDIX A

SPHERICAL VECTOR WAVE FUNCTION

If we set the electric and magnetic vector potentials outside an antenna on the $e^{j\omega t}$ time dependence as

$$\begin{bmatrix} \mathbf{F} \\ \mathbf{A} \end{bmatrix} = \sum_{n=0}^{\infty} \sum_{m=0}^n \sum_{e,o} \begin{bmatrix} -\eta^{1/2} a_{nm}^+ \\ j\eta^{-1/2} b_{nm}^+ \end{bmatrix} \hat{\mathbf{r}} \psi_{nm}^e \quad (32)$$

where $\psi_{nm}^e = \lambda_{nm}^{-1/2} kr \cdot h_n^{(2)}(kr) P_n^m(\cos\theta) \frac{\cos(m\phi)}{\sin(m\phi)}$, k is the wave number, $\lambda_{nm} = (1 + \delta_{m0}) 2\pi n(n+1)/(2n+1)$

$(n+m)!/(n-m)!$, and δ_{ij} is the Kronecker delta, then the electric and magnetic fields

$$\mathbf{E} = -\nabla \times \mathbf{F} + \frac{\eta}{jk} \nabla \times \nabla \times \mathbf{A} \quad (33)$$

$$\mathbf{H} = \nabla \times \mathbf{A} + \frac{1}{jk\eta} \nabla \times \nabla \times \mathbf{F} \quad (34)$$

yield (1) and (2), a linear combination of the spherical vector wave functions [8], [9]

$$\begin{aligned} \mathbf{M}_{nm\epsilon} &= \nabla \times \hat{\mathbf{r}}\psi_{nm\epsilon} \\ &= \lambda_{nm}^{-1/2} k \left\{ \hat{\boldsymbol{\theta}} \frac{m}{\sin \theta} h_n^{(2)}(kr) P_n^m(\cos \theta) \frac{-\sin(m\phi)}{\cos} \right. \\ &\quad \left. - \hat{\boldsymbol{\phi}} h_n^{(2)}(kr) \frac{\partial}{\partial \theta} P_n^m(\cos \theta) \frac{\cos(m\phi)}{\sin} \right\} \quad (35) \end{aligned}$$

$$\begin{aligned} \mathbf{N}_{nm\epsilon} &= \frac{1}{k} \nabla \times \nabla \times \hat{\mathbf{r}}\psi_{nm\epsilon} \\ &= \lambda_{nm}^{-1/2} k \left\{ \hat{\mathbf{r}} \frac{n(n+1)}{kr} h_n^{(2)}(kr) P_n^m(\cos \theta) \frac{\cos(m\phi)}{\sin} \right. \\ &\quad + \hat{\boldsymbol{\theta}} \frac{1}{kr} \frac{\partial}{\partial r} [r h_n^{(2)}(kr)] \frac{\partial}{\partial \theta} P_n^m(\cos \theta) \frac{\cos(m\phi)}{\sin} \\ &\quad \left. + \hat{\boldsymbol{\phi}} \frac{1}{kr} \frac{\partial}{\partial r} [r h_n^{(2)}(kr)] \frac{m}{\sin \theta} P_n^m(\cos \theta) \frac{-\sin(m\phi)}{\cos} \right\}. \quad (36) \end{aligned}$$

$\mathbf{M}_{nm\epsilon}^{(1)}$ and $\mathbf{N}_{nm\epsilon}^{(1)}$ in (8) are different from $\mathbf{M}_{nm\epsilon}$ and $\mathbf{N}_{nm\epsilon}$ in that $h_n^{(2)}(kr)$ is replaced by $j_n(kr)$, where $j_n(kr)$ is the spherical Bessel function of the first kind.

The fields of the antenna generating TE_{10} and TM_{10} modes are written as

$$\begin{aligned} \mathbf{E} &= \eta^{1/2} (a_{10}^+ \mathbf{M}_{10} + b_{10}^+ \mathbf{N}_{10}) \\ &= \eta^{1/2} k \sqrt{\frac{3}{8\pi}} \left\{ \hat{\mathbf{r}} 2b_{10}^+ \left[\frac{1}{(jkr)^2} + \frac{1}{(jkr)^3} \right] \cos \theta \right. \\ &\quad + \hat{\boldsymbol{\theta}} b_{10}^+ \left[\frac{1}{jkr} + \frac{1}{(jkr)^2} + \frac{1}{(jkr)^3} \right] \sin \theta \\ &\quad \left. - \hat{\boldsymbol{\phi}} j a_{10}^+ \left[\frac{1}{jkr} + \frac{1}{(jkr)^2} \right] \sin \theta \right\} e^{-jkr} \quad (37) \end{aligned}$$

$$\begin{aligned} \mathbf{H} &= j\eta^{-1/2} (a_{10}^+ \mathbf{N}_{10} + b_{10}^+ \mathbf{M}_{10}) \\ &= j\eta^{-1/2} k \sqrt{\frac{3}{8\pi}} \left\{ \hat{\mathbf{r}} 2a_{10}^+ \left[\frac{1}{(jkr)^2} + \frac{1}{(jkr)^3} \right] \cos \theta \right. \\ &\quad + \hat{\boldsymbol{\theta}} a_{10}^+ \left[\frac{1}{jkr} + \frac{1}{(jkr)^2} + \frac{1}{(jkr)^3} \right] \sin \theta \\ &\quad \left. - \hat{\boldsymbol{\phi}} j b_{10}^+ \left[\frac{1}{jkr} + \frac{1}{(jkr)^2} \right] \sin \theta \right\} e^{-jkr}. \quad (38) \end{aligned}$$

APPENDIX B

TE_{10} AND TM_{10} MODES UNDER COORDINATE ROTATIONS

The spherical mode under coordinate rotations as depicted in Fig. 1 can be derived from the following formula on the spherical harmonics [9]

$$Y_n^m(\theta, \phi) = \sum_{m'=-n}^n D_{m'm}^{(n)} Y_n^{m'}(\theta', \phi') \quad (39)$$

where

$$\begin{aligned} D_{m'm}^{(n)} &= e^{jm'\phi_1} \sqrt{\frac{(n+m')!(n-m)!}{(n+m)!(n-m)!}} \sum_{\sigma=0}^{n-m'} \\ &\quad \times \binom{n+m}{n-m'-\sigma} \binom{n-m}{\sigma} \\ &\quad \cdot (-1)^{n-m-\sigma} \left(\cos \frac{\theta_1}{2} \right)^{2\sigma+m'+m} \\ &\quad \times \left(\sin \frac{\theta_1}{2} \right)^{2n-2\sigma-m'-m} \quad (40) \end{aligned}$$

Y_n^m is the spherical harmonic function

$$Y_n^m = \sqrt{\frac{2n+1}{4\pi} \frac{(n-m)!}{(n+m)!}} P_n^m(\cos \theta) e^{jm\phi},$$

$Y_n^{-m} = (-1)^m Y_n^{m*}$. ϕ_1 and θ_1 are the rotation angles about the former z -axis and the new y -axis, respectively, as depicted in Fig. 1. For TE_{10} and TM_{10} modes, we can get from (39) with $D_{\pm 10}^{(1)} = \mp(1/\sqrt{2})e^{\pm j\phi_1} \sin \theta_1$ and $D_{00}^{(1)} = \cos \theta_1$

$$\begin{aligned} P_1(\cos \theta) &= \cos \theta_1 P_1(\cos \theta') \\ &\quad - \cos \phi_1 \sin \theta_1 P_1^1(\cos \theta') \cos \phi' \\ &\quad + \sin \phi_1 \sin \theta_1 P_1^1(\cos \theta') \sin \phi'. \quad (41) \end{aligned}$$

Applying (41) to (35), (36) and exchange of the original and rotated coordinates with $-\phi_1$ and $-\theta_1$ angles result in

$$\begin{aligned} \begin{bmatrix} \mathbf{M}_{10}(\mathbf{r}') \\ \mathbf{N}_{10}(\mathbf{r}') \end{bmatrix} &= \cos \theta_1 \begin{bmatrix} \mathbf{M}_{10}(\mathbf{r}) \\ \mathbf{N}_{10}(\mathbf{r}) \end{bmatrix} \\ &\quad + \cos \phi_1 \sin \theta_1 \begin{bmatrix} \mathbf{M}_{11}^e(\mathbf{r}) \\ \mathbf{N}_{11}^e(\mathbf{r}) \end{bmatrix} \\ &\quad + \sin \phi_1 \sin \theta_1 \begin{bmatrix} \mathbf{M}_{11}^o(\mathbf{r}) \\ \mathbf{N}_{11}^o(\mathbf{r}) \end{bmatrix} \quad (42) \end{aligned}$$

where $\mathbf{r}' = (r, \theta', \phi')$. We can see that arbitrary TE_{1m} and TM_{1m} modes can be represented as a TM_{10} and a TE_{10} mode in properly rotated coordinates, respectively.

APPENDIX C

ADDITION THEOREM UNDER COORDINATE TRANSLATION AND ROTATION

The addition theorem of the spherical vector wave functions under coordinate translation is given as [10, p. 595]

$$\begin{aligned} \mathbf{M}_{nm}(\mathbf{r}) &= \sum_{\nu=1}^{\infty} \sum_{\mu=-\nu}^{\nu} A_{\nu\mu, nm} \mathbf{M}_{\nu\mu}^{(1)}(\mathbf{r}') \\ &\quad + B_{\nu\mu, nm} \mathbf{N}_{\nu\mu}^{(1)}(\mathbf{r}') \quad (43) \end{aligned}$$

$$\begin{aligned} \mathbf{N}_{nm}(\mathbf{r}) &= \sum_{\nu=1}^{\infty} \sum_{\mu=-\nu}^{\nu} A_{\nu\mu, nm} \mathbf{N}_{\nu\mu}^{(1)}(\mathbf{r}') \\ &\quad + B_{\nu\mu, nm} \mathbf{M}_{\nu\mu}^{(1)}(\mathbf{r}') \quad (44) \end{aligned}$$

where $\mathbf{r} = \mathbf{r}' + \mathbf{r}_0$, $r' < r_0$.

$$\mathbf{M}_{nm} = c_{nm} \left[\mathbf{M}_{nm}^e + j\mathbf{M}_{nm}^o \right] \quad (45)$$

$$\mathbf{N}_{nm} = c_{nm} \left[\mathbf{N}_{nm}^e + j\mathbf{N}_{nm}^o \right] \quad (46)$$

where $c_{nm} = (-1)^m k^{-1} \sqrt{(1 + \delta_{m0})n(n+1)/2}$.

The general expressions for the translation coefficients, $A_{\nu\mu,nm}$ and $B_{\nu\mu,nm}$ are complicated, so we consider only the case of $n = 1$ and $m = 0$ in [13] as

$$A_{\nu\mu,10} = \frac{\sqrt{3}}{\nu} \sqrt{\frac{(\nu+\mu)(\nu-\mu)}{(2\nu-1)(2\nu+1)}} \alpha_{\nu-1,\mu,00} + \frac{\sqrt{3}}{\nu+1} \sqrt{\frac{(\nu+\mu+1)(\nu-\mu+1)}{(2\nu+1)(2\nu+3)}} \alpha_{\nu+1,\mu,00} \quad (47)$$

$$B_{\nu\mu,10} = \frac{j\mu\sqrt{3}}{\nu(\nu+1)} \alpha_{\nu\mu,00} \quad (48)$$

where $\alpha_{\nu\mu,00} = (-1)^{\nu+\mu} \sqrt{4\pi} Y_{\nu}^{-\mu}(\theta_0, \phi_0) h_{\nu}^{(2)}(kr_0)$.

The translation coefficients between TE_{10} , TM_{10} modes at origin and translated TE_{1m} , TM_{1m} modes centered at \mathbf{r}_0 are given by

$$A_{10,10} = P_0(\cos\theta_0)h_0^{(2)}(kr_0) + P_2(\cos\theta_0)h_2^{(2)}(kr_0) \quad (49)$$

$$B_{10,10} = 0 \quad (50)$$

$$A_{1,\pm 1,10} = \pm \sqrt{\frac{1}{8}} P_2^1(\cos\theta_0) e^{\mp j\phi_0} h_2^{(2)}(kr_0) \quad (51)$$

$$B_{1,\pm 1,10} = -j \sqrt{\frac{9}{8}} P_1^1(\cos\theta_0) e^{\mp j\phi_0} h_1^{(2)}(kr_0). \quad (52)$$

By some manipulations of (43) and (44), the similar form can be built on TE_{nm}^e , TM_{nm}^e modes, in which the translation coefficients between TE_{10} , TM_{10} modes and TE_{11}^e , TM_{11}^e modes can be written by

$$A_{11^e,10} = -j^0 \frac{1}{\sqrt{2}} (A_{11,10} \mp A_{1,-1,10}) = -\frac{1}{2} P_2^1(\cos\theta_0) \frac{\cos\phi_0}{\sin\phi_0} h_2^{(2)}(kr_0) \quad (53)$$

$$B_{11^e,10} = -j^1 \frac{1}{\sqrt{2}} (B_{11,10} \mp B_{1,-1,10}) = \pm \frac{3}{2} P_1^1(\cos\theta_0) \frac{\sin\phi_0}{\cos\phi_0} h_1^{(2)}(kr_0). \quad (54)$$

When the translated coordinate is rotated, the coefficients, $A_{\nu\mu,nm}$ and $B_{\nu\mu,nm}$ in (43) and (44) are replaced by $A'_{\nu\mu,nm}$ and $B'_{\nu\mu,nm}$ which are linear combinations of $A_{\nu\mu,nm}$ and $B_{\nu\mu,nm}$, respectively [9]. $A'_{10,10}$ and $B'_{10,10}$ are given from (42) as

$$\begin{bmatrix} A'_{10,10} \\ B'_{10,10} \end{bmatrix} = \cos\theta_1 \begin{bmatrix} A_{10,10} \\ B_{10,10} \end{bmatrix} + \sin\theta_1 \cos\phi_1 \begin{bmatrix} A_{11^e,10} \\ B_{11^e,10} \end{bmatrix} + \sin\theta_1 \sin\phi_1 \begin{bmatrix} A_{11^o,10} \\ B_{11^o,10} \end{bmatrix} \quad (55)$$

and written by

$$A'_{10,10} = \frac{3}{2} \cos\theta_1 \left\{ -\sin^2\theta_0 \frac{1}{jkr_0} + (3\cos^2\theta_0 - 1) \times \left[\frac{1}{(jkr_0)^2} + \frac{1}{(jkr_0)^3} \right] \right\} e^{-jkr_0} + \frac{3}{4} \sin\theta_1 \cos(\phi_1 - \phi_0) \sin 2\theta_0 \times \left\{ \frac{1}{jkr_0} + 3 \left[\frac{1}{(jkr_0)^2} + \frac{1}{(jkr_0)^3} \right] \right\} e^{-jkr_0} \quad (56)$$

$$B'_{10,10} = -j \frac{3}{2} \sin\theta_1 \sin(\phi_1 - \phi_0) \sin\theta_0 \times \left[\frac{1}{jkr_0} + \frac{1}{(jkr_0)^2} \right] e^{-jkr_0}. \quad (57)$$

REFERENCES

- [1] A. Kurs, A. Karalis, R. Moffatt, J. D. Joannopoulos, P. Fisher, and M. Soljacic, "Wireless power transfer via strongly coupled magnetic resonances," *Science*, vol. 317, no. 5834, pp. 83–86, Jul. 6, 2007.
- [2] Y. Kim and H. Ling, "Investigation of coupled mode behaviour of electrically small meander antennas," *Electron. Lett.*, vol. 43, no. 23, Nov. 2007.
- [3] A. Karalis, J. D. Joannopoulos, and M. Soljacic, "Efficient wireless non-radiative mid-range energy transfer," *Ann. Phys.*, vol. 323, no. 1, pp. 34–48, Jan. 2008.
- [4] J. E. Hansen, *Spherical Near-Field Antenna Measurements*. London: Peter Peregrinus, 1988, pp. 85–85.
- [5] W. K. Kahn and W. Wasylkiwskyj, "Coupling, radiation, and scattering by antennas," in *Proc. Symp. on Generalized Networks*, Brooklyn, NY, 1966, vol. 16, pp. 83–114.
- [6] W. Wasylkiwskyj and W. K. Kahn, "Scattering properties and mutual coupling of antennas with prescribed radiation pattern," *IEEE Trans. Antennas Propag.*, vol. 18, pp. 741–752, Nov. 1970.
- [7] W. Wasylkiwskyj and W. K. Kahn, "Theory of mutual coupling among minimum-scattering antennas," *IEEE Trans. Antennas Propag.*, vol. 18, pp. 204–216, Mar. 1970.
- [8] A. C. Gately, Jr, D. J. R. Stock, and B. R.-S. Cheo, "A network description for antenna problems," *Proc. IEEE*, vol. 56, pp. 1181–1193, Jul. 1968.
- [9] S. Stein, "Addition theorems for spherical wave functions," *Quart. Appl. Math.*, vol. 19, no. 1, pp. 15–24, 1961.
- [10] W. C. Chew, *Waves and Fields in Inhomogeneous Media*. New York: IEEE Press, 1995, pp. 595–595.
- [11] G. Gonzalez, *Microwave Transistor Amplifiers: Analysis and Design*, 2nd ed. NJ: Prentice-Hall, 1997, pp. 50–50.
- [12] D. M. Pozar, *Microwave Engineering*, 2nd ed. New York: Wiley, 1998.
- [13] W. C. Chew and Y. M. Wang, "Efficient ways to compute the vector addition theorem," *J. Electromagnet. Waves Appl.*, vol. 7, no. 5, pp. 651–665, 1993.



Jaechun Lee (S'05–M'08) received the B.S. degree from Soongsil University, Seoul, Korea, in 2000, and the M.S. and Ph.D. degrees from the Seoul National University, in 2002 and 2008, respectively, all in electronics/electrical engineering.

He is currently with Samsung Advanced Institute of Technology (SAIT), Yongin, Korea. His research interests include analysis/design of electromagnetic (EM) structures, antennas, and microwave active/passive circuits.



Sangwook Nam (S'87–M'88) received the B.S. degree from Seoul National University, Seoul, Korea, in 1981, the M.S. degree from the Korea Advanced Institute of Science and Technology (KAIST), in 1983, and the Ph.D. degree from the University of Texas at Austin, in 1989, all in electronics/electrical engineering.

From 1983 to 1986, he was a Researcher with the Gold Star Central Research Laboratory, Seoul, Korea. Since 1990, he has been with Seoul National University, where he is currently a Professor in the School of Electrical Engineering. His research interests include analysis/design of electromagnetic (EM) structures, antennas, and microwave active/passive circuits.